Structural aspects of amorphous iron(III) fluorides

1988 J. Phys. C: Solid State Phys. 21 1351

(http://iopscience.iop.org/0022-3719/21/8/011)

J. Phys. C: Solid State Phys. **21** (1988) 1351–1361. Printed in the UK

Structural aspects of amorphous iron(III) fluorides

J M Greneche†, A Le Bail‡, M Leblanc‡, A Mosset§, F Varret†, J Galy§ and G Ferey‡

† Laboratoire de Spectrométrie Mössbauer (Unitée Associée au CNRS 807), Université du Maine, F72017 Le Mans Cédex, France

‡ Laboratoire des Fluorures (Unitée Associée au CNRS 449), Université du Maine, F72017 Le Mans Cédex, France

§ Laboratoire de Chimie de Coordination, 205 route de Narbonne, 31400 Toulouse, France

Received 20 July 1987, in final form 7 September 1987

Abstract. Different forms of amorphous FeF_3 (a-FeF_3) are obtained either by vapour deposition or fluorination techniques. A structural investigation by extended x-ray absorption fine-structure spectroscopy and diffraction techniques (neutrons and x-rays) was undertaken in order to confirm and refine our previous Mössbauer data. The latter are summarised and compared with the data for the three crystalline forms of FeF_3. For both amorphous compounds, structural results agree with Mössbauer results; the trivalent iron ion is surrounded by weakly distorted fluorine octahedra and the Fe–F distances are estimated to be 1.95(1) Å. The a-FeF_3 obtained by fluorination is built up from only corner-sharing octahedra while the a-FeF_3 obtained by vapour deposition exhibits corner-sharing but perhaps also edge-sharing octahedra. Both compounds show speromagnetic behaviour evidenced by high-field Mössbauer spectroscopy. In comparison with the magnetic structures of the three crystalline phases of FeF_3, and in particular with their degree of frustration, one can describe 'ideal' a-FeF_3 as consisting of random corner-sharing octahedra where iron sites belong to odd- and even-membered cycles.

1. Introduction

Several ferric amorphous fluorides have been synthesised in the last ten years and their magnetic behaviour has been extensively investigated using Mössbauer spectroscopy by different groups (Ferey *et al* 1979a, b, Lachter *et al* 1980, Eibschutz *et al* 1981, 1984). Moreover, the isothermal and non-isothermal crystallisation kinetics, mainly of amorphous FeF_3 (a-FeF_3), has been studied using Mössbauer spectroscopy and neutron diffraction (Lopez-Herrera 1983, 1984, Leblanc *et al* 1985a, Greneche *et al* 1986a, 1987b).

The present study is focused on two forms of a-FeF_3 which are obtained either by the vapour deposition technique on a cold substrate (a-FeF_3) or by the soft chemistry reaction of HF gas on crystalline $FeCl_3$ (a-FeF_3.xHF). Until now, few results concerning structural aspects have been obtained on such compounds because of various difficulties; these materials are never pure, and either a small amount of divalent iron is observed after the deposition process or an HF contribution is induced during fluorination. In contrast the reproducibility of these compounds is very sensitive to the experimental conditions of the preparation and leads to major problems in the vapour deposition

0022-3719/88/081351 + 11 $02.50

technique where each run yields only a small amount of material. In addition, these compounds are highly hygroscopic.

The aim of this paper is to describe the structural investigations performed on a-FeF_3 and a-FeF_3. xHF by extended x-ray absorption fine-structure spectroscopy (EXAFS), neutrons diffraction and large-angle x-ray scattering (LAXS) experiments; then their structural aspects are discussed in comparison with those of crystalline FeF_3 forms and fluoride glasses. In § 2 the Mössbauer results are briefly reported.

2. Summary of Mössbauer studies

The results which are mentioned here originate mainly from our previous Mössbauer investigations of a-FeF_3. xHF given by Greneche *et al* (1987c). The hyperfine data for the two a-FeF_3 compounds are very similar and show that the trivalent iron belongs to weakly distorted octahedra of fluorine atoms. The hyperfine field distribution is very close to a symmetric Gaussian shape with a low-field tail; moreover, the positive and negative electric field gradients at iron sites are distributed with equal probability. Their spin-freezing temperatures were estimated by Mössbauer thermal scanning and susceptibility measurements; the T_G values are very similar as shown on table 1. Moreover, they are lower than those of rhombohedral FeF_3 (r-FeF_3) and hexagonal tungsten bronze FeF_3 (HTB FeF_3) (Leblanc *et al* 1985b, 1986) but higher than that of pyrochlore FeF_3 (pyr-FeF_3) (Ferey *et al* 1986). A similar evolution of the low-temperature hyperfine field values can be seen in table 1. The different values of the magnetic ordering temperature are well explained by the degree of frustration of the magnetic structure of crystalline compounds evidenced by neutron diffraction (Ferey *et al* 1986). Figure 1 shows typical Mössbauer spectra recorded at liquid-helium temperature under an applied field parallel to the γ-beam for crystalline and amorphous forms of FeF_3. The broadening of the outer lines is characteristic of the absence of rotation of the magnetic moments under the applied field; such an effect is consistent with a non-collinear antiferromagnetic structure for HTB FeF_3 (spectrum B) and pyr-FeF_3 (spectrum C) and with a speromagnetic behaviour for a-FeF_3 (spectra D and E), in contrast with the r-FeF_3 which exhibits a spectrum (spectrum A) typical of a collinear antiferromagnetic structure. From this, one can conclude that there is magnetic frustration in a-FeF_3, which could be consistent with the *ab initio* models of a random network made up of odd- and even-membered rings of corner-sharing octahedra (Coey and Murphy 1982, Greneche *et al* 1986b, 1987a).

Table 1. Magnetic ordering temperature, hyperfine field values (at 4.2 K) and densities of a-FeF_3 and crystalline FeF_3. The values in brackets show the accuracy.

	T_N or T_G (K)	H_{hyp} (kOe)	ρ_{exp} (g cm^{-3})	ρ_{calc} (g cm^{-3})
a-FeF_3	39 (2)	560 (2)	2.90 (20)	—
a-FeF_3.0.4HF	36 (2)	550 (2)	2.80 (20)	—
r-FeF_3	363 (2)	618 (2)	3.60 (5)	3.61
HTB FeF_2	105 (2)	577 (2)	—	3.11
HTB FeF_3.$\frac{1}{3}H_3O$	129 (2)	560 (2)	3.25 (10)	3.33
pyr-FeF_3	22 (1)	517 (2)	—	2.74

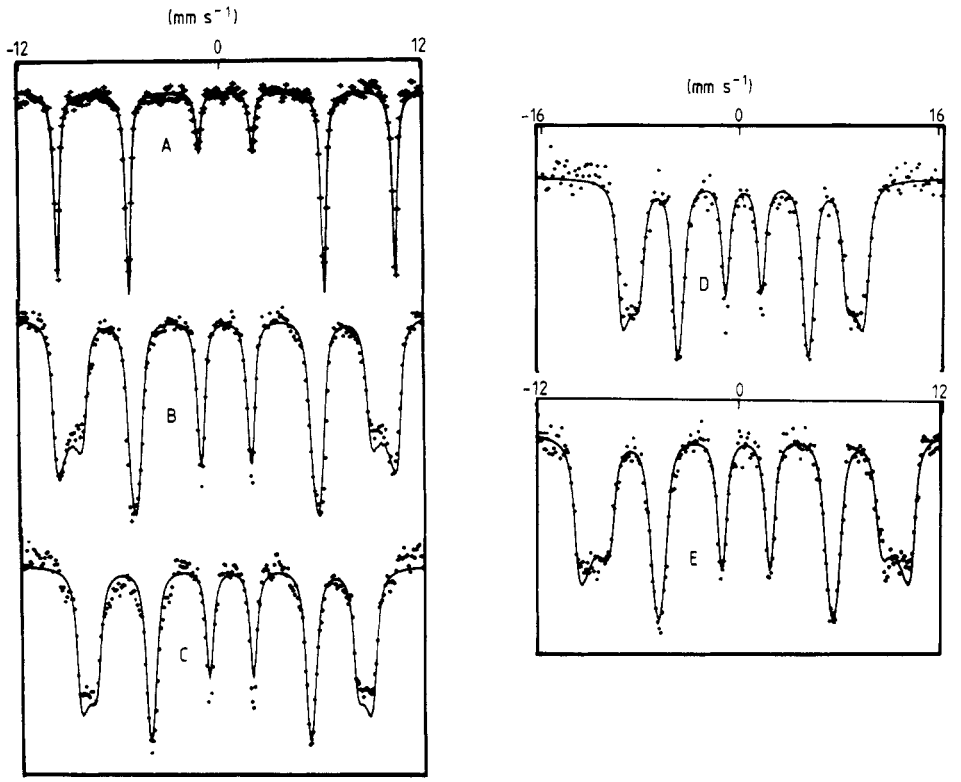

Figure 1. Mössbauer spectra recorded at 4.2 K under an external magnetic field parallel to the γ-beam on r-FeF_3 (70 kG) (spectrum A), HTB FeF_3 (60 kG) (spectrum B), pyr-FeF_3 (40 kG) (spectrum C), a-FeF_3 (60 kG) (spectrum D) and a-FeF_3.0.8HF (70 kG) (spectrum E).

3. Density measurements

Owing to the hygroscopic character of the powdered samples, the density measurements were performed in ethyl phthalate after pumping under vacuum for 12 h at room temperature.

The measured values are reported in table 1 and compared with those of the crystalline phases of FeF_3. The densities of the a-FeF_3 compounds are probably underestimated because of the small size of the particles. Despite the poor accuracy, one can conclude that the densities of the a-FeF_3 compounds are lower than those of the r-FeF_3 and HTB FeF_3 but higher than that of pyr-FeF_3.

4. Extended x-ray absorption fine-structure spectroscopy

The local environment of the iron atoms was investigated for both a-FeF_3 forms by EXAFS and compared with that of the three crystalline forms of FeF_3. Absorption spectra were recorded at room temperature at the Laboratoire d'Utilisation du Rayonnement

Electromagnétique. All the samples were made of powder placed between two boron nitride discs. The data were refined by a standard method described by Le Bail *et al* (1984). We report briefly the main steps as follows.

(i) The EXAFS modulations $\chi(k)$ were determined using a k^3 correction to take into account the large decrease in the retrodiffusion fluorine amplitude.

(ii) The modulus $|F(R)|$ of the Fourier transform of $f(k) = k^3\chi(k)$ was evaluated.

(iii) The partial functions $f_j(k)$ associated with the j-coordinated spheres were calculated by inverse Fourier transformation of $F(r)$.

(iv) Refinement of the mean distances R_j and the standard deviation σ_j of the distance distribution were obtained from the following equation proposed by Stern *et al* (1980):

$$f_j(k) = (k/R_j)^2 N_j S_0^2(k) T_j(k) \exp(-2\sigma_j^2 k^2) \exp[-2(R_j - \Delta)/\lambda] \sin[2kR_j + \varphi_j(k)]$$

where λ is the mean free path of the electrons and $\Delta = R_1$.

The EXAFS modulations $\chi(k)$ with the k^3 correction and the modulus $|F(R)|$ corrected for phase shifts in the case of Fe–F pairs of the crystalline and amorphous forms of FeF_3 are presented in figure 2 and the refined data are given in table 2.

The iron ion is confirmed to be sixfold coordinated in the a-FeF_3 forms. The Fe–F distances are very close to those known in fluorine glasses (Le Bail *et al* 1983, 1984), as shown in table 2, and to those observed in the crystalline forms of FeF_3. The Fe–Fe

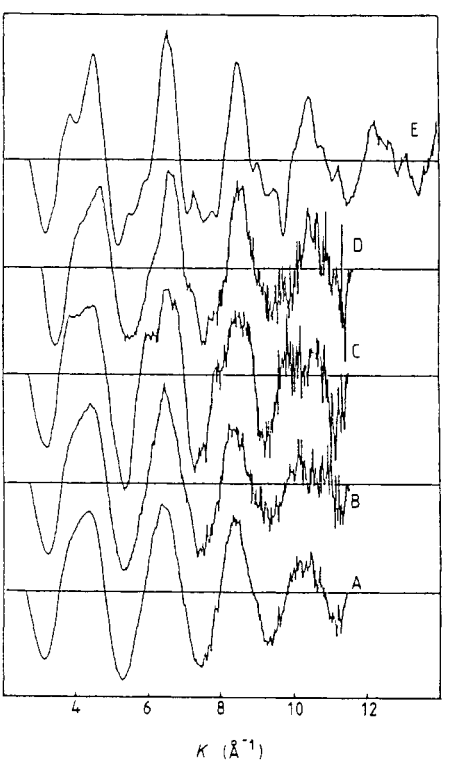

Figure 2. $k^3\chi(k)$ curves for a-FeF_3 (spectrum A), a-FeF_3.0.4HF (spectrum B), pyr-FeF_3 (spectrum C), HTB FeF_3 (spectrum D) and r-FeF_3 (spectrum E).

Table 2. Fe–F distances in crystalline, amorphous or glassy iron fluorides (indicated by g-) with the standard deviation of the distance distribution and the corresponding coordination number of Fe^{3+} deduced from EXAFS data. The coordination number of 6.0 for r-FeF_3, HTB FeF_3 and pyr-FeF_3 was fixed during the refinement. The Fe–F distances in parentheses for r-FeF_3, HTB FeF_3 and pyr-FeF_3 were deduced from x-ray diffraction at 300 K, 4.2 K and 2.5 K, respectively.

	Fe–F (Å)	σ_{Fe-F} (Å)	N
a-FeF_3	1.95 ± 0.01	0.07	6.2 ± 1
a-FeF_3.0.4HF	1.95 ± 0.01	0.08	6.4 ± 1
r-FeF_3	1.93 ± 0.01 (1.992)	0.05	6.0 ± 1
HTB FeF_3	1.94 ± 0.01 (1.913)	0.06	6.0 ± 1
pyr-FeF_3	1.95 ± 0.01 (1.926)	0.07	6.0 ± 1
g-$PbMnFeF_7$	1.92 ± 0.01	0.05	5.7 ± 1
g-$PbCuFeF_7$	1.93 ± 0.01	0.07	6.6 ± 1
g-$BaCuFeF_7$	1.93 ± 0.01	0.08	6.5 ± 1
g-$BaMnFeF_7$	1.93 ± 0.01	0.08	6.0 ± 1

distances can be estimated from the second peak in the crystalline spectra; in the a-FeF_3 compounds, as illustrated in figure 3, the second peak is too weak to provide the Fe–Fe distances without any ambiguity.

From the XANES spectra reported in figure 4, one can conclude that all samples show a weak pre-peak characteristic of the forbidden 1s → 3d transition, confirming that all the FeF_3 varieties are made up of weakly distorted octahedra.

5. Diffraction studies: results and discussion

5.1. Neutron diffraction

Neutron diffraction patterns of FeF_3.0.4HF and a-FeF_3 were recorded using the D1B and D2 diffractometers, respectively, of the Institut Laue–Langevin, Grenoble. The experimental conditions are as follows: a-FeF_3.0.4HF (D1B diffractometer), λ = 2.519 Å, $10° < 2\theta < 90°$, T = 2, 50, 150 and 300 K; a-FeF_3 (D2 diffractometer), λ = 1.22 Å, $2.4° < 2\theta < 123°$, T = 5, 30 and 300 K.

The magnetic correlation functions $dm(r)$ were estimated with an arbitrary scale from the following equation:

$$dm(r) \propto \int_0^{Q_{max}} QI_m(Q) \sin rQ \, dQ$$

where $I_m(Q)$ is the pure magnetic interference function established by a simple difference (an example is given by Le Bail *et al* (1983)) between two spectra obtained below and above, respectively, the spin-freezing temperature and Q_{max} was taken to be equal to 3.8 Å (figure 5). It should be noted that this simple treatment is expected to give the true solution only if there is no correlation between the magnetic moment direction and that

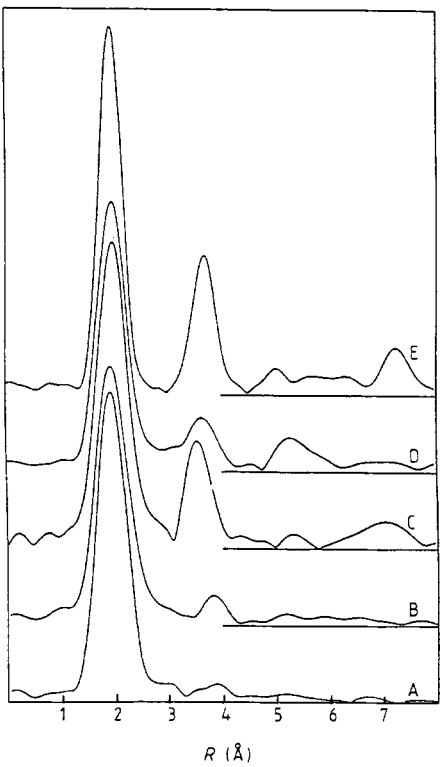

Figure 3. Radial distribution functions for a-FeF_3 (spectrum A), a-FeF_3.0.4HF (spectrum B), pyr-FeF_3 (spectrum C), HTB FeF_3 (spectrum D) and r-FeF_3 (spectrum E).

of the vector ***r***; otherwise the system has an infinite number of solutions (Le Bail *et al* 1983). Keeping in mind this fact, we estimated the Fe–Fe distances (reported in table 3) from $dm(r)$. The Fe–Fe(1) and Fe–Fe(2) distances (first- and second-nearest neighbour) were attributed to the first 'antiferromagnetic peak' and the second 'ferromagnetic peak', respectively (figure 6).

For a-FeF_3.xHF, the room-temperature spectrum was not considered because of the large inelastic contribution of hydrogen diffusion. A corner-sharing octahedra situation is observed from the results for a-FeF_3.xHF, which are in agreement with all those known for fluoride glasses such as $PbTM^{2+}TM^{3+}F_7$ where $TM^{2+} \equiv Mn^{2+}$ or Zn^{2+} and $TM^{3+} \equiv Fe^{3+}$ or Ga^{3+} (Le Bail *et al* 1983).

Curiously, for the a-FeF_3, the Fe–Fe distances were found to be shorter and an evolution was observed between 5 and 30 K. The smaller value of the Fe–Fe distance (2.99 Å) is not likely to occur frequently for corner-sharing octahedra. On the contrary, it could suggest the presence of some edge-sharing octahedra for which the ideal distance should be 2.76 Å. However, two experimental facts are not consistent with such an assumption: first, the drastic thermal variation in the Fe–Fe distance between 30 and 5 K (between 2.99 and 3.24 Å) seems to be too large in such a temperature range unless the compound changes 'structure' between 30 and 5 K; secondly, it is well known that 90° superexchange interactions (corresponding to edge-sharing octahedra) occur over a considerably smaller distance than do 180° interactions (corner-sharing octahedra)

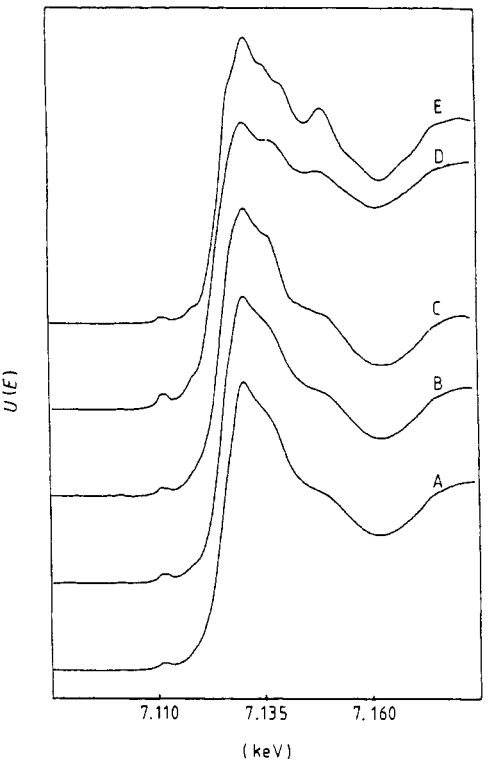

Figure 4. XANES spectra of a-FeF_3 (spectrum A), a-FeF_3.0.4HF (spectrum B), pyr-FeF_3 (spectrum C), HTB FeF_3 (spectrum D) and r-FeF_3 (spectrum E).

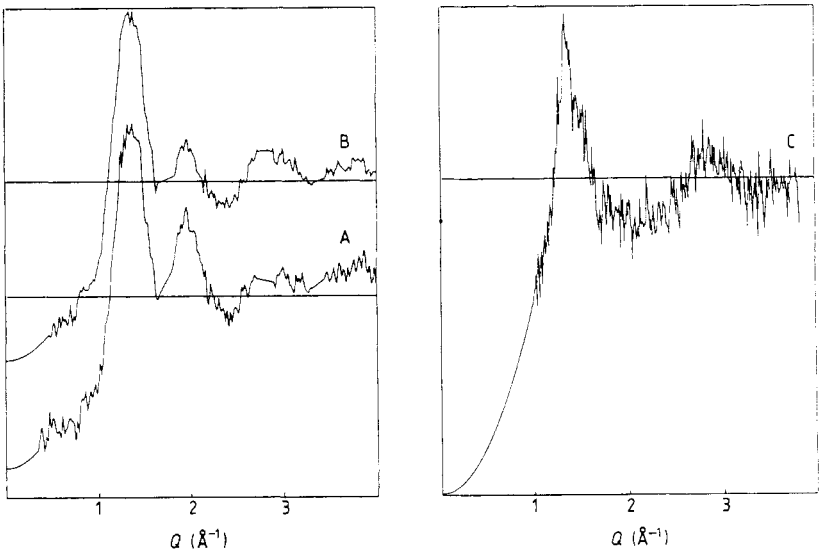

Figure 5. Magnetic difference spectra of neutron diffraction for a-FeF_3 between 30 and 150 K (spectrum A) and between 5 and 300 K (spectrum B) and a-FeF_3.0.4HF between 2 and 150 K (spectrum C).

Table 3. Neutron diffraction results.

	Temperature (K)	Fe–Fe(1) (Å)	Fe–Fe(2) (Å)
$FeF_3.0.4HF$	2–150	3.62	5.08
FeF.0.4HF	50–150	3.55	5.04
VD FeF_3	5–300	3.24	5.37
VD FeF_3	30–300	2.99	5.22

(Goodenough 1963). If such a number of edge-sharing octahedra exist in a-FeF_3, its freezing temperature should be much lower than that of the a-FeF_3.xHF in which only corner-sharing octahedra are present. It is not the case since the T_G values are 39 and 36 K for the a-FeF_3 and the a-FeF_3,xHF respectively. These inconsistencies lead to some doubts about the above treatment of the magnetic data.

Experiments were especially designed for the neutron magnetic study (large wavelength); however, the nuclear part of the spectrum may be used in order to perform the calculation of the atomic distribution function for VD a-FeF_3 (as already mentioned, this is not possible for a-FeF_3.xHF because of the high hydrogen content). The nuclear interference function $I(Q)$ was derived from the intensities $I_a(Q)$ (normalised in a classical way (Le Bail *et al* 1985)) following the usual formula:

$$I(Q) = [I_a(Q) - \langle b^2\rangle - \langle b\rangle^2)]/\langle b\rangle^2.$$

A small amount of r-FeF_3 (3 wt%) was detected and the Bragg diffraction peaks were removed by interpolation; also a decrease in the intensities at large Q-values was

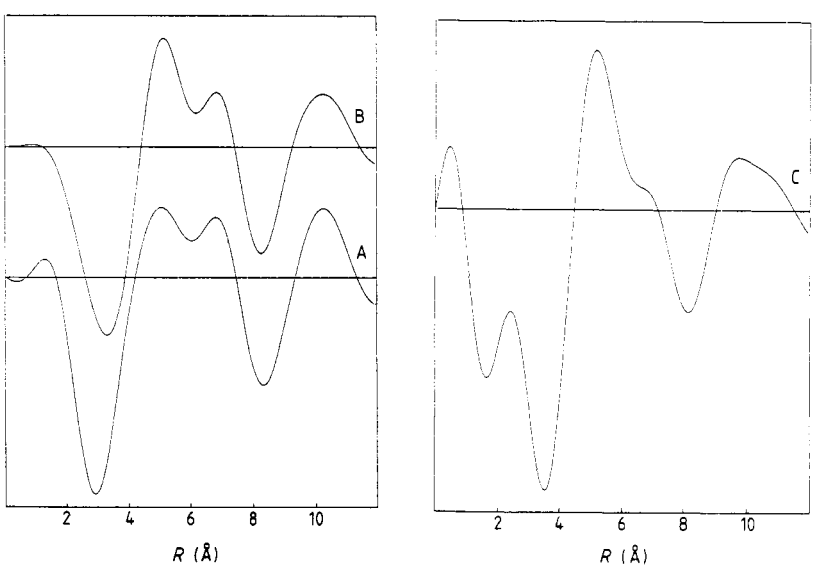

Figure 6. Magnetic radial distribution functions established from differences in neutron diffraction spectra for VD a-FeF_3 between 30 and 300 K (curve A) and between 5 and 300 K (curve B) and for a-FeF_3.0.4HF between 2 and 150 K (curve C).

observed that could not be due to the Fe^{3+} magnetic form factor (at room temperature in the paramagnetic region). This latter effect was clearly due to the presence of hydrogen induced during the preparation of the basic crystalline compound for the vapour deposition method; intensities were then corrected (following Dubois *et al* (1982)) and the hydrogen content was estimated to be 2 mol%.

The reduced interference function $I(Q) - 1$ is shown in figure 7(*a*). The reduced atomic distribution function $G(R)$ (figure 7(*b*)) was determined according to

$$G(R) = \frac{2}{\pi}\int_0^{Q_{max}} Q[I(Q) - 1]M(Q)\sin QR \, dQ$$

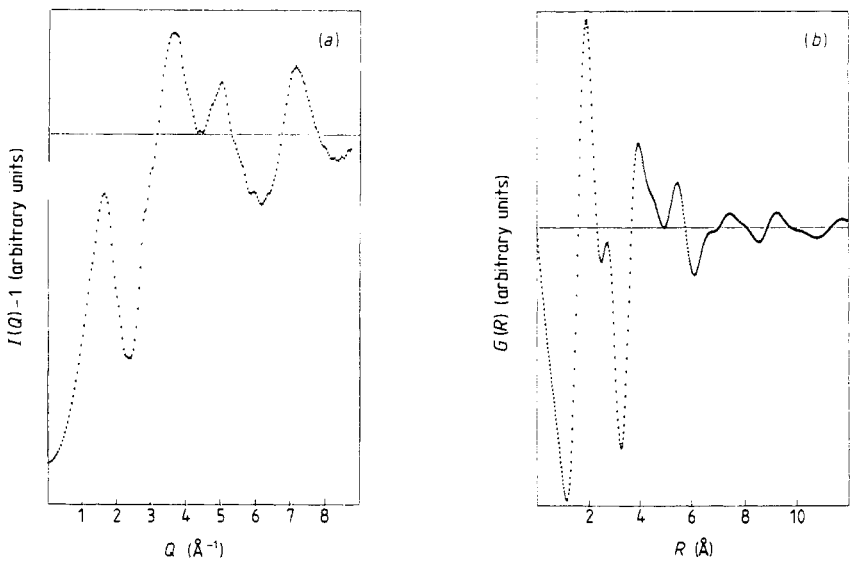

Figure 7. (*a*) Interference function and (*b*) reduced atomic distribution function for a-FeF_3 deduced from neutron experiments at room temperature.

where $M(Q)$ is the modification function due to Lorch (1969) applied in order to remove truncation effects. The first two peaks near 1.95 and 2.75 Å on $G(R)$ presented in figure 7(*b*) can be attributed unambiguously to Fe–F and F–F first neighbours. An attempt was made to determine the coordination number by a Gaussian peak-fitting technique on the radial distribution function using the previous estimated density (2.9) but the result leads to 4.3 fluorine atoms around the iron atom which is not consistent with results given by EXAFS and Mössbauer spectroscopy. In order to obtain a coordination number of 6, it was found necessary to increase the density value to 3.5 which is close to that of r-FeF_3. A large underestimation of the density for the a-FeF_3 varieties is not unexpected because of the extremely high specific surface of these finely divided materials.

5.2. *Large-angle x-ray scattering*

The samples consisted of powder platelets 0.3–0.7 mm thick (of the a-FeF_3 and a-

$FeF_3.xHF$) obtained under pressure and placed between two dried Mylar foils 10 μm thick. The diffuse spectra scattered by such samples irradiated with graphite-monochromated Mo Kα radiation were obtained by using an automatic diffractometer and were collected in the range $1° < \theta < 66°$ (where 2θ is the angle diffusion) (Lecante *et al* 1985). All the measurements were carried out at room temperature in transmission geometry.

The scattered intensities were corrected for polarisation and absorption effects to give $I_c(s)$ and then normalised. The reduced intensities $i(s)$ were calculated as follows:

$$I(Q) - 1 = KI_c(s) - \sum_i n_i[(f_i(s) + \Delta f_i')^2 + \Delta f_i''^2 + I_i(s)]$$

where K is the normalisation factor, n_i is the number of atoms i in the unit volume, $f_i(s)$ is the atomic scattering factor (taken from tables published by Cromer and Waber (1974)), $\Delta f_i'$ and $\Delta f_i''$ are the real and imaginary part of the anomalous dispersion and $I_i(s)$ is the total incoherent radiation for the atom i.

The interference function and the corresponding reduced atomic distribution function $G(R)$ are established for the a-$FeF_3.xHF$ and are presented in figures 8(a) and 8(b),

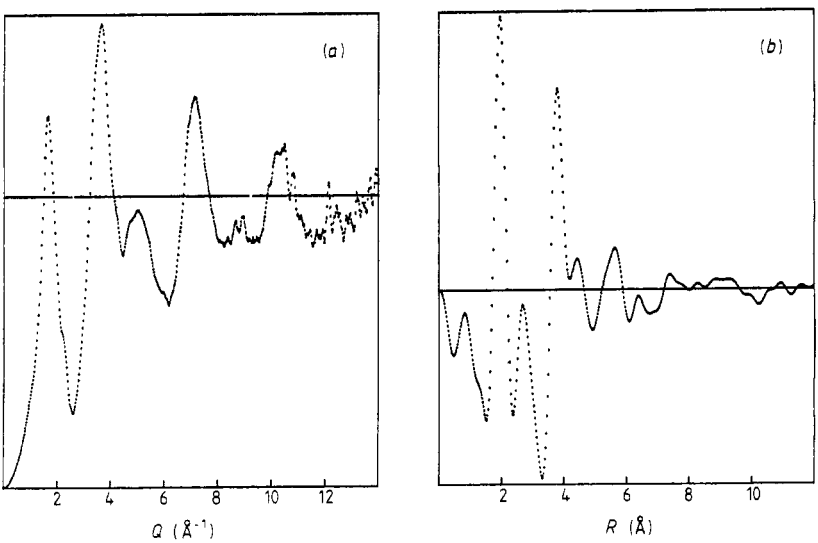

Figure 8. (a) Interference function and (b) reduced atomic distribution function for a-FeF_3.0.4HF deduced from LAXS experiments at room temperature.

respectively. The two well defined peaks evidenced at 1.95(1) Å and 2.75(1) Å on $G(R)$ can be attributed to Fe–F and F–F nearest neighbours, respectively; this confirms that the octahedra are weakly distorted. Two peaks are also observed between 3.80 and 4.45 Å but cannot be attributed unambiguously; they probably are the result of two contributions: Fe–Fe first-nearest neighbours and Fe–F second-nearest neighbours.

In contrast, no results were obtained on the a-FeF_3 as a result of partial crystallisation induced during the platelet preparation.

6. Conclusion

These structural investigations on a-FeF_3 and a-$FeF_3.x$HF carried out using several techniques agree with previous Mössbauer results and sometimes refine them. They led to the following conclusions: the iron is sixfold coordinated (EXAFS and neutron diffraction), the octahedra are weakly distorted (XANES) and the Fe–F distance is estimated to 1.95(1) Å (EXAFS, LAXS and neutron diffraction). The Fe–Fe distances seem to be in agreement with octahedra shared by corners. The same structural characteristics are observed in fluoride glasses. In addition, the hyperfine parameters and the magnetic structure are very similar for both varieties of a-FeF_3.

These new observations are consistent with the earlier Mössbauer results, suggesting an 'ideal FeF_3' composed of corner-sharing octahedra with odd- and even-membered rings and resulting in a speromagnetic behaviour.

The following difficulties encountered during the present study should be noted: the small size of particles when measuring the density which is a determinant parameter to improve structural models, the hygroscopic character from any experimental point of view and the presence of hydrogen in the neutron investigations.

References

Coey J M D and Murphy P J K 1982 *J. Non-Cryst. Solids* **50** 125
Cromer D T and Waber J T 1974 *International Tables for X-ray Crystallography* vol IV (Birmingham: Kynoch) table 2.2.a
Dubois J M, Chieux P, Le Caer G, Schweizer J and Bletry J 1982 *J. Physique Coll.* **43** C9 23
Eibschutz M, Lines M E, Van Uitert L G, Guggenheim H J and Zydzik G J 1981 *Phys. Rev.* B **24** 2343
—— 1984 *Phys. Rev.* B **29** 3843
Ferey G, de Pape R, Leblanc M and Pannetier J 1986 *Rev. Chim. Miner.* **23** 474
Ferey G, Leclerc A M, de Pape R, Mariot J P and Varret F 1979a *Solid State Commun.* **29** 477
Ferey G, Varret F and Coey J M D 1979b *J. Phys. C: Solid State Phys.* **12** L531
Goodenough J B 1963 *Magnetism and the Chemical Bond* (New York: Interscience)
Greneche J M, Leblanc M, Varret F and Ferey G 1986a *Hyperfine Interact.* **27** 317
Greneche J M, Teillet J and Coey J M D 1986b *J. Non-Cryst. Solids* **83** 27
—— 1987a *J. Physique* **48** 1709
Greneche J M, Varret F, Leblanc M and Ferey G 1987b *Solid State Commun.* **61** 813
—— 1987c *Solid State Commun.* **63** 435
Lachter A, Gianduzzo J C, Barriere A S, Fournes L and Menil F 1980 *Phys. Status Solidi* a **61** 619
Le Bail A, Jacoboni C and de Pape R 1983 *J. Solid State Chem.* **48** 168
—— 1984 *J. Solid State Chem.* **52** 32
—— 1985 *J. Non.Cryst. Solids* **74** 205
Leblanc M, Ferey G, Greneche J M, Le Bail A, Varret F, de Pape R and Pannetier J 1985a *J. Physique Coll.* **46** C8 175
Leblanc M, Ferey G, Pannetier J and de Pape R 1985b *Rev. Chim. Miner.* **22** 107
Leblanc M, Pannetier J, de Pape R and Ferey G 1986 *Solid State Commun.* **58** 171
Lecante P, Mosset A and Galy J 1985 *J. Appl. Crystallogr.* **18** 214
Lopez-Herrera M E 1983 *Thesis* University of Le Mans
Lopez-Herrera M E, Varret F, Calage Y and Ferey G 1984 *J. Magn. Magn. Mater.* **44** 304
Lorch E A 1969 *J. Phy. C: Solid State Phys.* **2** 229
Stern E A, Bunker B A and Heald S M 1980 *Phys. Rev.* B **21** 5521